Other workers report charge transfer corresponding to a single hcp layer.[9] Unfortunately, the uncertainty in the coulometry in the present experiment was too large to substantiate this point.

The STM image is not necessarily a representation of only the metal atoms on the surface, as the presence of adsorbed anions could also contribute to the image. The changes shown in Figure 4 were not observed when the potential of the working electrode was swept in the same range in a solution free of lead ions. However, since the potential of zero charge (PZC) shifts about 400 to 500 mV in the negative direction upon the deposition of lead, the adsorption of anions would be enhanced on the lead-covered surface vs the lead-free surface.

The use of tunneling microscopy to study monolayer deposition on an electrode surface is very new, and much work is needed before the STM images can be explained definitively. Nevertheless, it is clear that this technique will be able to make a unique contribution to the study of electrode surfaces.

(8) Juttner, K.; Siegenthaler, H. *Electrochim. Acta* **1978**, *23*, 971.
(9) Bewick, A.; Thomas, B. *J. Electroanal. Chem.* **1975**, *65*, 911.

Summary

It has been demonstrated that scanning tunneling microscopy can be an effective in situ technique to study the very early stages of electrodeposition. In situ scanning tunneling microscopy results have indicated that the underpotential deposition of lead on Au(111) is accompanied by an overall smoothing of the surface features and an increase in the size of the flat terraces. The first of these changes has been attributed to a shift in the potential of zero charge in the negative direction after underpotential deposition which would enhance the specific adsorption of nitrate on the surface. The increase in the size of the terraces results evidently from the adsorption of lead atoms on a lead adlayer at the periphery of the terraces.

Acknowledgment. We thank Rex Wright and Lloyd Lacomb for help with the image processing. This research was partially supported by NSF Grant DMR-84-14569, DOE Grant AC03-82-ER-13000, and DARPA Contract N00014-85-K-0388.

Solute-Dependent Solvent Force Constants for Ion Pairs and Neutral Pairs in a Polar Solvent

Emily A. Carter[†] and James T. Hynes*

Department of Chemistry and Biochemistry, University of Colorado, Boulder, Colorado 80309-0215
(Received: January 23, 1989)

The solvent force constants k characterizing the fluctuations of a polar solvent in the presence of a solute ion pair A^+B^- and a neutral pair AB are determined by molecular dynamics simulation. The origin of the observed difference in the k values and the consequences for electron-transfer rate–reaction free energy gap behavior are discussed.

Introduction

In the presence of an immersed solute, a polar solvent continuously fluctuates due to the translational and reorientational motions of its constituent molecules. The concept of a (harmonic) free energy curve governing these fluctuations as a function of a solvent coordinate plays a central role in many aspects of solvation dynamics; examples include electron-transfer reactions,[1] time-dependent fluorescence,[2] and heavy particle charge transfers such as S_N2 reactions.[3] With a few exceptions,[3-6] it is usually assumed that the force constant k characterizing the curvature of the well in this free energy curve is independent of the charge distribution of the solute; the standard dielectric continuum Marcus theory[1] for electron transfers provides a well-known illustration. In a recent series of papers, Kakitani and Mataga (KM) and co-workers[4-6] have argued that k should instead strongly increase with increasing solute charge, and they have predicted significant consequences of this for rate–energy gap behavior for various classes of photochemical electron-transfer reactions. Here we present the first molecular dynamics (MD) computer simulations addressed to this question. Solvation free energy curves for an ion pair (IP) A^+B^- and a corresponding neutral pair (NP) AB in a model polar solvent are found, and the associated solvent force constants are defined and determined to differ for the IP and the NP. The origin of the difference and some consequences for electron-transfer rates are briefly described.

Formulation

A convenient microscopic level choice of a solvent coordinate is[1,7,8] ΔE, the difference of the potential energy of a given set of solvent molecule configurations in the presence of the IP and NP:

$$\Delta E = V_{\text{solv,IP}} - V_{\text{solv,NP}} \tag{1}$$

In the limit where the short-range nonelectrostatic solute–solvent interactions are identical for the IP and NP, the collective coordinate ΔE is determined exclusively by the electrostatic Coulomb interactions and reduces to the Coulomb interaction energy of the IP solute with the polar solvent molecules in their given configurations. In the point dipole approximation for the solvent molecules, ΔE would reduce to

$$\Delta E = -\int d\mathbf{r}\, \mathbf{P}(\mathbf{r})\cdot[\mathbf{E}^\circ_A(\mathbf{r}-\mathbf{r}_A) + \mathbf{E}^\circ_B(\mathbf{r}-\mathbf{r}_B)] \tag{2}$$

where $\mathbf{P}(\mathbf{r})$ is the solvent orientational polarization at $\mathbf{r}$ and $\mathbf{E}^\circ_i(\mathbf{r}$

[†] Permanent address: Department of Chemistry and Biochemistry, University of California, Los Angeles, CA 90024-1569.

(1) Marcus, R. A. *Annu. Rev. Phys. Chem.* **1964**, *15*, 155. (b) Newton, M. D.; Sutin, N. *Annu. Rev. Phys. Chem.* **1984**, *35*, 437. (c) Hynes, J. T. *J. Phys. Chem.* **1986**, *90*, 3701.
(2) Hynes, J. T.; van der Zwan, G. *J. Phys. Chem.* **1985**, *89*, 4181.
(3) (a) Gertner, B. J.; Bergsma, J. P.; Wilson, K. R.; Lee, S.; Hynes, J. T. *J. Chem. Phys.* **1987**, *86*, 1377. (b) Lee, S.; Hynes, J. T. *J. Chem. Phys.* **1988**, *88*, 6853.
(4) (a) Kakitani, T.; Mataga, N. *Chem. Phys.* **1985**, *93*, 381. (b) Kakitani, T.; Mataga, N. *J. Phys. Chem.* **1985**, *89*, 4752. (c) Kakitani, T.; Mataga, N. *J. Phys. Chem.* **1985**, *89*, 8.
(5) (a) Kakitani, T.; Mataga, N. *J. Phys. Chem.* **1986**, *90*, 993. (b) Kakitani, T.; Mataga, N. *J. Phys. Chem.* **1987**, *91*, 6277.
(6) (a) Kakitani, T.; Mataga, N. *Chem. Phys. Lett.* **1986**, *124*, 437. (b) Hatano, Y.; Saito, M.; Kakitani, T.; Mataga, N. *J. Phys. Chem.* **1988**, *92*, 1008.
(7) Warshel, A. *J. Phys. Chem.* **1982**, *86*, 2218.
(8) (a) Hwang, J. K.; Warshel, A. *J. Am. Chem. Soc.* **1987**, *109*, 715. (b) Kuharski, R. A.; Bader, J. S.; Chandler, D.; Sprik, M.; Klein, M. L.; Impey, R. W. *J. Chem. Phys.* **1988**, *89*, 3248.

0022-3654/89/2093-2184$01.50/0

$-\mathbf{r}_i$) is the vacuum electric field at $\mathbf{r}$ due to ion i at $\mathbf{r}_i$ in the IP. This is the conventional dielectric continuum limit solvent coordinate.[9] In this Letter, however, we retain the full microscopic definition of ΔE (eq 1).

When the solvent is in equilibrium with a given solute pair (SP), ΔE will fluctuate such that a probability distribution of numerical values Δe of the microscopic variable ΔE will be observed, reflecting the different solvent molecule configurations:

$$P_{SP}(\Delta e) = \langle \delta[\Delta e - \Delta E] \rangle_{SP} \quad (3)$$

Here δ denotes the delta function and the brackets indicate an equilibrium average in the presence of the solute pair. Fourier representation of the delta function and a second-order cumulant expansion[10] reduce this to a Gaussian distribution

$$P_{SP}(\Delta e) = [2\pi\langle(\delta\Delta E)^2\rangle_{SP}]^{1/2} \exp\left[\frac{-(\delta\Delta e)^2}{2\langle(\delta\Delta E)^2\rangle_{SP}}\right] \quad (4)$$

where the δ notation indicates that the equilibrium average value is subtracted, e.g., $\delta\Delta E = \Delta E - \langle\Delta E\rangle_{SP}$. This in turn defines the harmonic solvent free energy in the presence of the SP via $P_{SP}(\Delta e) \propto \exp[-G(\Delta e)/k_BT]$ as

$$G_{SP}(\Delta e) = G_{SP}^{eq}(\Delta e_{SP}^{eq}) + \tfrac{1}{2}k_{SP}(\Delta e - \Delta e_{SP}^{eq})^2; \quad k_{SP} = k_BT/\langle(\delta\Delta E)^2\rangle_{SP} \quad (5)$$

by which we identify the solvent force constant k_{SP} in terms of the fluctuations of ΔE in the presence of the SP. (Note that fluctuations in ΔE are well-defined in the presence of the NP, i.e., even though the IP is absent, since the solvent configurations in the presence of the NP fluctuate and change ΔE.) Both our results described within and previous simulations[6b,8] indicate that the harmonic approximation is quite good.

It will prove important subsequently to define the solvent frequency $\omega_{SP} = (k_{SP}/m_{SP})^{1/2}$, where m_{SP} is the average mass associated with ΔE. This mass is defined through the equipartition theorem

$$\tfrac{1}{2}\langle(\Delta\dot{E})^2\rangle_{SP} = k_BT/2m_{SP} \quad (6)$$

involving the velocity $(\Delta\dot{E})$.

Computer Simulation Results

MD simulations were conducted for model IP and NP species in a model polar solvent. The solvent is composed of 342 rigid dipolar molecules with constituent atoms of mass 40 au separated from each other by a fixed distance of 2.0 Å and with partial point charges $\pm q$ such that the dipole moment is 2.4 D. The number density is 0.012 Å^{-3} and the temperature is 250 K. (This solvent is a rough caricature of methyl chloride.) The constituent members of the IP A^+B^- and the NP AB each have a mass of 40 au and are rigidly separated by 3.0 Å. The total potential energy of interaction consists of Lennard-Jones and Coulomb potentials $V(r_{ij}) = V_{LJ}(r_{ij}) + Z_iZ_jr_{ij}^{-1}$ between each atomic site with Z_i the charge on site i. The LJ parameters are $\epsilon/k_B = 200$ K and $\sigma = 3.5$ Å for each site in the solvent molecules and the SP. With these definitions, ΔE in eq 1 has only Coulombic contributions, since the IP and NP differ only by the presence of the point charges in the former.

Constant-temperature[11] MD simulations were carried out in a periodically replicated cubic box with sides of length 30.52 Å. The integration of the equations of motion was effected with the Verlet algorithm[12] and a time step of 10^{-14} s. The long-range forces were treated by using the Ewald summation method,[13] and the bond constraints were implemented via the SHAKE algorithm.[14a]

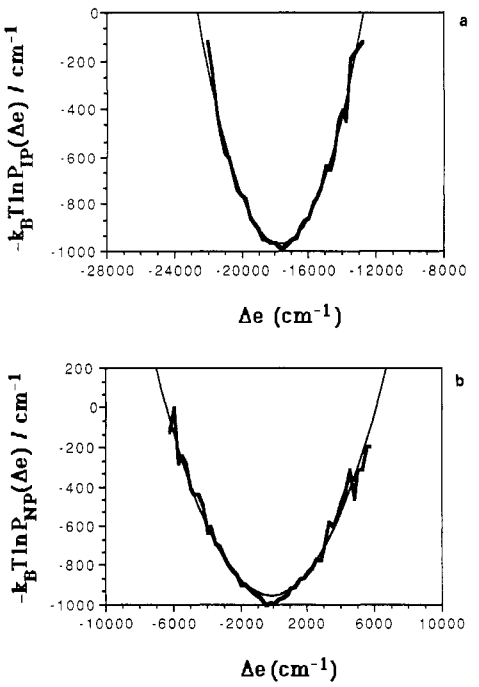

Figure 1. MD results for solvent free energy curves $-k_BT \ln P_{SP}(\Delta e)$ (cf eq 3) versus numerical values Δe of ΔE (thick solid lines): (a) ion pair A^+B^- solute; (b) neutral pair AB solute. Parabolic fits to the free energies are indicated by the thin solid lines.

The probability distributions (eq 3) were obtained for each SP case via the construction of Δe histograms in runs of 410 ps after an equilibration period of 10 ps. The free energy curves extracted from these are shown in Figure 1. The solvent force constants determined from polynomial fits to these are $k_{IP} = 8.0 \times 10^{-5}$ cm and $k_{NP} = 4.9 \times 10^{-5}$ cm. (These are in good agreement with the values separately extracted via the second member of eq 5 of 8.2×10^{-5} and 5.3×10^{-5} cm, respectively. Errors are estimated to be ±10% from 205 statistically independent samples of $(\Delta E)^2$ in the 410-ps interval and from the Gaussian character of ΔE.) The solvent frequencies $\omega_{SP} = [\langle(\Delta\dot{E})^2\rangle_{SP}/\langle(\delta\Delta E)^2\rangle_{SP}]^{1/2}$ are determined in the simulations to be $\omega_{IP} = 5.6$ ps^{-1} and $\omega_{NP} = 5.0$ ps^{-1}.

Discussion

The present MD finding of an increased solvent force constant for the charged IP compared to the NP case ($k_{IP}/k_{NP} = 1.6$) is qualitatively consistent with the proposals[4-6] of Kakitani and Mataga (KM). It is also in line with the idea that the restriction of the solvent molecules due to the charges in the IP reduces the fluctuations in ΔE compared to the NP case and, according to eq 5, increases the solvent force constant.

This is a nonlinear effect in the following sense. First recall from eq 5 that $k_{SP}^{-1} \propto \langle(\delta\Delta E)^2\rangle_{SP}$. Since the potential energy of interaction of the polar solvent with the IP differs by ΔE (eq 1) from that with the NP, we have

$$\langle(\delta\Delta E)^2\rangle_{IP} = \langle e^{-\Delta E/k_BT}\rangle_{NP}^{-1}\langle(\delta\Delta E)^2 e^{-\Delta E/k_BT}\rangle_{NP}$$

$$= \langle(\Delta E)^2\rangle_{NP} + \frac{1}{2(k_BT)^2}[\langle(\Delta E)^4\rangle_{NP} - 3\langle(\Delta E)^2\rangle_{NP}^2] + \ldots \quad (7)$$

Thus, k_{IP} equals k_{NP} only for sufficiently small $\Delta E/k_BT$ values (to be expected, e.g., for large SP species). We note that only small deviations from Gaussian probability distributions result from the observed different spring constants; for example, the non-Gaussian fluctuation term bracketed in the final member of eq 7 is inferred to be only about $10^{-2}\langle(\Delta E)^2\rangle_{NP}^2$ in magnitude.

(9) (a) Zusman, L. D. *Chem. Phys.* **1980**, *49*, 295. (b) Calef, D. F.; Wolynes, P. G. *J. Phys. Chem.* **1983**, *87*, 3387.
(10) Kubo, R. *J. Math. Phys.* **1963**, *4*, 174.
(11) Nosé, S. *J. Chem. Phys.* **1984**, *81*, 511.
(12) Verlet, L. *Phys. Rev.* **1967**, *159*, 98.
(13) Hansen, J. P. In *Molecular Dynamics Simulation of Statistical Mechanical Systems*; Ciccotti, G., Hoover, W., Eds.; North-Holland: New York, 1986.
(14) (a) Ciccotti, G.; Ryckaert, J. P. *Comput. Phys. Rep.* **1986**, *4*, 345. (b) Ciccotti, G.; Ferrario, M.; Hynes, J. T.; Kapral, R. *Chem. Phys.* **1989**, *129*, 241.

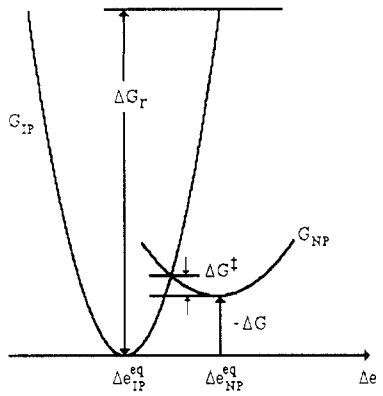

Figure 2. Schematic free energy diagram for the NP → IP interconversion AB → A^+B^- indicating the activation free energy, $\Delta G^\ddagger$, the reorganization energy, $\Delta G_r = G_{IP}(\Delta e = 0) - G_{IP}(\Delta e^{eq}_{IP})$, and the reaction free energy, $\Delta G = G^{eq}_{IP} - G^{eq}_{NP}$.

In a dielectric continuum or point dipole solvent description, such nonlinearities could be interpreted as dielectric saturation[6] for the solvent polarization $\mathbf{P}(\mathbf{r})$ (cf. eq 2). However, the evident lack of molecular level significance for this (point dipole) solvent polarization for finite size dipolar solvent molecules[15] and the importance of local solvent structural effects[16] suggest that the dielectric saturation concept should be applied only with considerable caution.

We mention in passing that electrical fluctuations for water solvent in the presence of small positively charged and uncharged spheres have recently been determined in an MD simulation by Maroncelli and Fleming (MF).[15] While no force constants were examined in that work, application of our eq 5 to the MF results indicates that the solvent force constant for water *decreases* as the solute charge increases. This trend, which is opposite to that found here and in Monte Carlo simulation results[6] for spherical ions in a solvent of point dipoles in spherical hard cores, may be related to the special hydrogen-bonding properties of water and deserves further study.

As emphasized by KM,[4-6] the solute charge dependence of solvent force constants can have considerable impact on electron-transfer rate–free energy gap relations. This is illustrated by Figure 2, from which one readily derives the activation free energy relation

$$\Delta G^\ddagger = \beta\{[(1+\beta)\Delta G_r]^{1/2} - [\beta\Delta G_r - \Delta G]^{1/2}\}^2 \qquad (8)$$

for the NP → IP reaction (in the *absence* of internal modes) in terms of the IP reorganization energy, ΔG_r, the reaction free energy, $\Delta G = G^{eq}_{IP} - G^{eq}_{NP}$, and the force constant parameter $\beta = k_{NP}/(k_{IP} - k_{NP})$, which is $\beta = 1.6$ in the present case. For very small β, $\Delta G^\ddagger$ grows much more slowly, $\Delta G^\ddagger \approx \beta[(\Delta G_r)^{1/2} - (-\Delta G)^{1/2}]^2$, with increasing free energy gap $-\Delta G$ than does the standard equal force constant ($\beta = \infty$) Marcus result[1] $\Delta G^\ddagger_{MAR} = (\Delta G_r + \Delta G)^2/4\Delta G_r$; the small curvature of the NP free energy is responsible for this feature. This tends to suppress the so-called "anomalous region" for the rate of exothermic reactions.[1,4] The contrast between eq 8 and $\Delta G^\ddagger_{MAR}$ is illustrated in Figure 3a in a charge separation rate constant context. $\Delta G^\ddagger$ becomes effectively infinite at $\beta\Delta G_r = \Delta G$; in this endothermic case, the NP free energy curve falls below the IP curve as the latter slides up compared to the former, and there is no longer an intersection. For the reverse (charge recombination) reaction $A^+B^- \rightarrow$ AB with reaction free energy $\Delta G_{rec} = G^{eq}_{NP} - G^{eq}_{IP} = -\Delta G$, one has

$$\Delta G^\ddagger_{rec} = \Delta G_{rec} + \beta\{[(1+\beta)\Delta G_r]^{1/2} - [\beta\Delta G_r + \Delta G_{rec}]^{1/2}\}^2 \qquad (9)$$

illustrated in Figure 3b. In the extreme limit $\beta \rightarrow 0$, $\Delta G^\ddagger_{rec}$ reduces to ΔG_{rec} for $\Delta G_{rec} > 0$ and is effectively infinity when $\Delta G_{rec} < 0$. This behavior reflects the sliding of the flat NP free energy curve vertically with respect to the IP curve in Figure 2; when

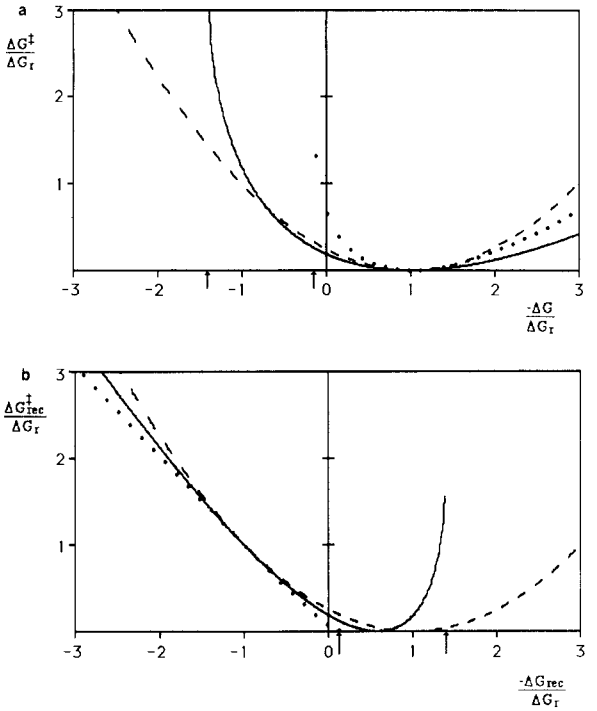

Figure 3. Activation free energy, $\Delta G^\ddagger$ ($\Delta G^\ddagger_{rec}$), versus negative reaction free energy, $-\Delta G$ ($-\Delta G_{rec}$), for the charge separation (recombination) reaction, both normalized by ΔG_r, the reorganization energy: (a) AB → A^+B^-; (b) A^+B^- → AB. Legend: (—) present $\beta = k_{NP}/(k_{IP} - k_{NP})$ value = 1.6; (– – –) $\beta = \infty$ (Marcus theory); (···) $\beta = 0.16$. Arrows indicate points on the abscissa where the activation free energy is effectively infinite (see text). The activation free energies for $\beta = 0.16$ have been multiplied by a factor of 10 in (a).

$\Delta G_{rec} < 0$, the two curves no longer intersect (for $\beta = 0$).

The trends noted above for $\Delta G^\ddagger$ have been discussed by KM for charge separation and recombination reactions.[4-6] It is noteworthy, however, that KM typically employ β values approximately 1 order of magnitude or more less than that found here ($\beta = 1.6$).

KM suggest that different solvent force constant effects will also be present for charge shift reactions[5] such as $A^-B \rightarrow AB^-$. But for identical A and B species, there can be no difference between the solvent force constants in ΔE free energy curves, by symmetry, and the Marcus result $\Delta G^\ddagger_{MAR}$ applies in our description. We note that the collective variable ΔE refers to both donor and acceptor species simultaneously. Thus, for the charge shift reaction, as well as for charge separations and recombinations, ΔE represents a single mode that is coupled simultaneously to the donor and acceptor centers. By contrast, the KM formulation[4-6] is based on the Hopfield treatment[17] using a Forster–Dexter formalism,[18] which assumes[19,20] that the donor and acceptor centers are coupled to different independent modes. This latter assumption for solvent modes in electron-transfer reactions has been extensively criticized by Jortner.[20] Simulations in which A and B have large separation such that a two-mode description could be appropriate would be of interest.

The KM analysis[4-6] is often couched in terms of differences in solvent frequencies rather than solvent force constants. Our results show that while the latter indeed depend on the solute charge state, the solvent frequencies ω_{IP} and ω_{NP} are nearly identical (5.6 and 5.0 ps^{-1}, respectively). This compensation arises from the increase in the solvent mass associated with ΔE (eq 6), accompanying the increase in the force constant on going from the NP to the IP. One consequence of this near constancy in ω_{SP} for solute pairs is that the entropy change for e.g., the charge

(15) Maroncelli, M. P.; Fleming, G. R. *J. Chem. Phys.* **1988**, *89*, 5044.
(16) Morita, T.; Ladanyi, B. M.; Hynes, J. T. *J. Phys. Chem.*, in press.
(17) Hopfield, J. J. *Proc. Natl. Acad. Sci. U.S.A.* **1974**, *71*, 3640.
(18) (a) Forster, T. *Naturwissenschaften* **1946**, *33*, 166. (b) Dexter, D. L. *J. Chem. Phys.* **1953**, *21*, 836.
(19) Soules, T. F.; Duke, C. B. *Phys. Rev. B* **1971**, *3*, 262.
(20) Jortner, J. *J. Chem. Phys.* **1976**, *64*, 4860.

separation reaction $AB \rightarrow A^+B^-$

$$\Delta S = k_B \ln \omega_{NP}/\omega_{IP} \quad (10)$$

will be nearly zero, in contrast to estimates[4,5] of ΔS based solely on force constant ratios. Another consequence is that the prefactor $(\omega_{SP}/2\pi)$ in the transition state theory expression[1] for electron-transfer rates should depend only weakly on the charge distribution state of the reactant pair; an opposite conclusion would follow if only force constants were considered.

Finally, the solute charge dependence of the solvent force constants has marked consequences for the predicted spectral features of time-dependent fluorescence;[2] this will be discussed elsewhere.[21]

Acknowledgment. Acknowledgment is made to the donors of the Petroleum Research Fund, administered by the American Chemical Society, for partial support of this work. This work was also supported in part by NSF Grants CHE84-19830 and CHE88-07852. We gratefully acknowledge a grant of supercomputer time from the Pittsburgh Supercomputer Center. We thank Professor G. Ciccotti and Dr. D. A. Zichi for helpful discussions and Dr. M. Ferrario for providing the initial computer program, which was subsequently modified to perform this work. We are also grateful to Mr. Greg Smith for graphical assistance.

(21) Carter, E. A.; Hynes, J. T., to be submitted for publication.

Sites of Electron Trapping in DNA As Determined by ESR of One-Electron-Reduced Oligonucleotides

William A. Bernhard

Department of Biophysics, University of Rochester, Rochester, New York 14642 *(Received: October 31, 1988)*

The ESR spectrum of one-electron-reduced d(pApGpCpT) in a 12 M LiCl glass at 4 K is simulated using spectra of the four free radical anions: $T^{\bullet-}$, $C^{\bullet-}$, $A^{\bullet-}$, and $G^{\bullet-}$. Approximately 80% of the trapped electrons reside on cytosine, $C^{\bullet-}$. Changing the solute to a 1:1 mixture of d(pTpCpGpApCpG):d(pApGpCpTpGpC) increases the proportion of $C^{\bullet-}$ to ~87%. At temperatures below 78 K, cytosine is the dominate site of electron trapping in these oligonucleotides and, it is suggested, may be the dominant site in DNA as well.

Introduction

DNA exposed to the direct effects of ionizing radiation undergoes chemical changes that originate primarily from sites that have either lost or gained an electron. Determining the chemical nature and distribution of the damaged sites is a central problem in the field of radiation biology. Perhaps the most tractable part of this complex problem is determining the sites of electron attachment.

The most widely accepted model, at the present, is that at temperatures of 77 K and below electrons are trapped predominantly (or exclusively) at thymine (T) and holes are trapped at guanine (G). The evidence for this comes from ESR studies of DNA fibers,[1,2] ESR of DNA and its components in frozen aqueous solution,[3] ESR of nuclei acids in aqueous glasses,[4,5] pulse radiolysis,[6] and molecular orbital calculations.[7] This model has been adopted and is being used as a basis for modeling the mechanisms by which single-strand and double-strand breaks occur in DNA.[8] But difficulties with the $T^{\bullet-}/G^{\bullet+}$ model of direct damage in DNA have been apparent for some time. Gräslund et al. in their early work on fiber DNA were unable to eliminate C as a site that traps electrons, in addition to T.[1] Sevilla et al., studying dinucleoside phosphate in 12 M LiCl, concluded that the pyrimidines are more electron affinic than purines but could not exclude the possibility that cytosine's affinity was comparable to thymine. Also in that work, it was suggested that the preferential protonation of $T^{\bullet-}$ skews the ultimate trapping toward T.[5] By use of single-crystal ESR it was found that in a co-crystal of AdR:BrU, where the purine and pyrimidine bases are stacked, electron addition to A is stable at 77 K; no evidence of electron transfer from AdR to BrU was found.[9] In summary, there is evidence that electron attachment to the pyrimidine bases is more probable than to the purine bases, but the relative distribution among the four bases is unknown.

Our objective is to determine the distribution of electron capture among the bases at low temperature, <78 K. Information on the low-temperature trapping should provide insight into both the relative electron affinities of the four bases and the possibility of electron transfer between bases.

Methods

Oligonucleotides were purchased from Sigma Chemical Co. and Pharmacia Molecular Biologicals and used without further purification. The 12 M LiCl glasses were prepared by dissolving ~5 OD 260 units of oligomer in 5 μL of H_2O and mixing with 5 μL of 24 M LiCl. A 2-μL aliquot was reserved for optical density measurements, and the remaining 8-μL sample was injected into a 1.0 mm thin wall Spectrosil quartz tube for ESR measurements. The sample was quickly cooled to 2 K and X-irradiated at 50 keV for 15 min to a dose of 250 krad, and Q-band ESR spectra were recorded at 4 K. With the use of a calibrated ruby standard,[10] the free-radical concentration was found to be

(1) Gräslund, A.; Ehrenberg, A.; Rupprecht, A.; Ström, G. *Int. J. Radiat. Biol.* **1975**, *28*, 313.
(2) Hüttermann, J.; Voit, K.; Oloff, H.; Köhnlein, W.; Gräslund, A.; Rupprecht, A. *Faraday Discuss. Chem. Soc.* **1984**, *78*, 135.
(3) Gregoli, S.; Olast, J.; Bertinchamps, A. J. *Radiat. Res.* **1982**, *89*, 238.
(4) Sevilla, M. D.; Failor, R.; Clark, C.; Holroyd, R. A.; Petti, M. *J. Phys. Chem.* **1976**, *80*, 353.
(5) Sevilla, M. D.; D'Arcy, J. B.; Morehouse, K. M.; Engelhardt, M. L. *Photochem. Photobiol.* **1979**, *29*, 37.
(6) Adams, G. E.; Greenstock, C. L.; van Hemmen, J. J.; Willson, R. L. *Radiat. Res.* **1972**, *49*, 85.
(7) Berthod, H.; Gressner-Prettre, C.; Pullman, T. *Theor. Chim. Acta* **1966**, *5*, 53.
(8) Symons, M. C. R. *J. Chem. Soc., Faraday Trans. 1* **1987**, *83*, 1.
(9) Kar, L.; Bernhard, W. *Radiat. Res.* **1983**, *93*, 232.
(10) Bernhard, W. A.; Fouse, G. W. *Magn. Reson.*, in press.

0022-3654/89/2093-2187$01.50/0